Neuron, Vol. 30, 183–196, April, 2001, Copyright ©2001 by Cell Press

# Functional Interaction of the Active Zone Proteins Munc13-1 and RIM1 in Synaptic Vesicle Priming

**Andrea Betz,[1,5,6] Pratima Thakur,[2,5] Harald J. Junge,[1,5] Uri Ashery,[2,5,7] Jeong-Seop Rhee,[2,5] Volker Scheuss,[2] Christian Rosenmund,[2,4] Jens Rettig,[2,3,4] and Nils Brose[1,4]**

[1] Max-Planck-Institut
für experimentelle Medizin
Abteilung Neurogenetik
AG Molekulare Neurobiologie
Hermann-Rein-Str. 3
D-37075 Göttingen

[2] Max-Planck-Institut
für biophysikalische Chemie
Abteilung Membranbiophysik
Am Faßberg 11
D-37077 Göttingen

[3] Physiologisches Institut
Universität des Saarlandes
D-66421 Homburg/Saar
Germany

## Summary

**Synaptic neurotransmitter release is restricted to active zones, where the processes of synaptic vesicle tethering, priming to fusion competence, and $Ca^{2+}$-triggered fusion are taking place in a highly coordinated manner. We show that the active zone components Munc13-1, an essential vesicle priming protein, and RIM1, a Rab3 effector with a putative role in vesicle tethering, interact functionally. Disruption of this interaction causes a loss of fusion-competent synaptic vesicles, creating a phenocopy of Munc13-1-deficient neurons. RIM1 binding and vesicle priming are mediated by two distinct structural modules of Munc13-1. The Munc13-1/RIM1 interaction may create a functional link between synaptic vesicle tethering and priming, or it may regulate the priming reaction itself, thereby determining the number of fusion-competent vesicles.**

## Introduction

In contrast to most other secretory processes, synaptic neurotransmitter release is restricted to designated release sites. These so-called active zones are electron-dense regions of the presynaptic plasma membrane at which the final steps of synaptic vesicle exocytosis take place with extreme spatial and temporal accuracy. Typically, a presynaptic bouton contains hundreds of vesicles that cluster in close proximity of the active zone. A subpopulation of vesicles in this cluster is tethered specifically to the plasma membrane at the active zone. These tethered vesicles have to mature to a fusion-competent, primed state before an increase of the intracellular $Ca^{2+}$ concentration can trigger their fusion. Usually, only a small fraction of tethered vesicles in any given synapse is primed to fusion competence and ready to fuse in response to the $Ca^{2+}$ trigger. The size of this readily releasable vesicle pool determines synaptic release probability and signaling capacity (Südhof, 1995; Zucker, 1996).

Given their central role in late exocytotic steps of the synaptic vesicle cycle, active zones must contain the specific protein machinery that is responsible for vesicle tethering, priming, and fusion. However, the protein composition of active zones is largely unknown, and the two plasma membrane proteins that are thought to be involved in the vesicle fusion reaction, Syntaxin and SNAP-25, are not specific for active zones but rather distributed widely over the axonal plasma membrane (Garcia et al., 1995). Thus, the restriction of synaptic secretion to active zones is likely to be caused by regulatory mechanisms that act upstream of vesicle fusion. Such mechanisms include the targeted transport and clustering of vesicles in the axon terminal as well as the active zone-specific processes of tethering and priming.

Recently, four proteins with a specific localization to active zones have been identified: Piccolo/Aczonin (Wang et al., 1999; Fenster et al., 2000), RIM1 (Wang et al., 1997), Munc13-1 (Betz et al., 1998), and Bassoon (tom Dieck et al., 1998). The four proteins are tightly bound to the presynaptic cytoskeletal matrix and were detected at active zones of conventional synapses and, in the case of RIM1 and Bassoon, at presynaptic ribbons of synapses in the retina. Piccolo/Aczonin and Bassoon are very large (>400 kDa) homologous multidomain proteins with unknown function (tom Dieck et al., 1998; Wang et al., 1999; Fenster et al., 2000). RIM1 is a 180 kDa protein that shares homology with Piccolo/Aczonin and Bassoon in a short N-terminal sequence as well as in an N-terminal zinc finger structure (Wang et al., 1997). Like Piccolo/Aczonin, RIM1 contains a PDZ domain and two $C_2$ domains. The N-terminal zinc fingers of RIM1 and its homolog RIM2 bind to Rab3A and other Rab3 proteins in their GTP-bound state (Wang et al., 1997; Ozaki et al., 2000; Wang et al., 2000). One function of Rab3 binding to RIM1 and RIM2 may be to target and tether Rab3-GTP bearing synaptic vesicles to the active zone. Additional RIM functions may be linked to a cAMP-dependent guanyl nucleotide exchange factor (cAMP-GEFII; Ozaki et al., 2000). Among the four known active zone constituents, Munc13-1, a mammalian homolog of *Caenorhabditis elegans* UNC-13, is the only protein to which a defined function in the synaptic vesicle cycle was assigned. It is a 200 kDa brain-specific protein and represents a novel target of the diacylglycerol second messenger pathway that acts in parallel with protein kinase C to regulate neurotransmitter release (Betz et al., 1998). In glutamatergic synapses, Munc13-1 is an

[4] To whom correspondence should be addressed (e-mail: brose@em.mpg.de [N. B.], jrettig@med-rz.uni-sb.de [J. R.], crosenm@gwdg.de [C. R.]).

[5] These authors contributed equally to this work.

[6] Present address: Department of Molecular Biology, Princeton University, Princeton, New Jersey 08544.

[7] Present address: Tel Aviv University, Faculty of Life Sciences, Department of Neurobiochemistry, Tel Aviv 69978, Israel.

essential component of the synaptic vesicle priming apparatus. Munc13-1-deficient synapses are morphologically normal but do not contain fusion-competent vesicles (Augustin et al., 1999b).

Munc13-1 may mediate its priming effect by binding to the synaptic plasma membrane protein Syntaxin (Betz et al., 1997; Brose et al., 2000). In the presynaptic terminal, Syntaxin is present in two mutually exclusive complexes. First, Syntaxin forms a high-affinity complex with Munc18, which keeps Syntaxin in a closed conformation and prevents it from interaction with other proteins (see Misura et al., 2000, for the crystal structure of this complex and for a review of relevant literature). Second, Syntaxin in its open conformation forms a thermodynamically very stable complex with the plasma membrane protein SNAP25 and the synaptic vesicle protein Synaptobrevin/VAMP, the so-called "core complex" whose formation was suggested to represent a key step of secretory vesicle priming and/or of the fusion reaction itself (Sutton et al., 1998; Weber et al., 1998). Structural data as well as numerous in vitro studies suggest that a mechanism must exist that dissociates the Syntaxin/Munc18 complex or alters the conformation of its components in order to allow Syntaxin to participate in core complex formation. As Munc13-1 binds to an N-terminal sequence of Syntaxin that is also involved in Munc18 binding to Syntaxin (Betz et al., 1997; Sassa et al., 1999), Munc13-1 was suggested to promote core complex formation by displacing the negative regulator of complex assembly, Munc18, from Syntaxin, thereby stabilizing the open form of Syntaxin (Sassa et al., 1999; Brose et al., 2000). Alternatively, Munc13-1 may alter the conformation of Syntaxin and/or Munc18 in the Syntaxin/Munc18 complex via a direct interaction and thus promote core complex formation (Misura et al., 2000).

In the present study, we sought to identify molecular mechanisms by which the vesicle priming protein Munc13-1 is functionally integrated into the protein machinery of the active zone. We present biochemical and physiological evidence for a functional interaction between the active zone components Munc13-1 and RIM1.

## Results

### An Evolutionary Conserved N Terminus in a Novel Ubiquitously Expressed Munc13-2 Splice Variant

All three known rat Munc13 isoforms (Munc13-1, Munc13-2, and Munc13-3) are brain-specific proteins that share a common, highly homologous C-terminal region with $C_1$, $C_2$, and Munc13 homology domains but have unrelated N termini (Figure 1B; Koch et al., 2000). Recently, Song et al. (1998) identified a human Munc13 protein (hMunc13) in kidney (GenBank accession number AF020202). hMunc13 is homologous to rat Munc13-1 in its N terminus, while its C terminus is closely related to rat Munc13-2.

In order to determine if hMunc13 is a novel Munc13 isoform or a splice variant of one of the three known Munc13 gene products, we cloned its rat homolog. The deduced amino acid sequence of the cloned protein (GenBank accession number AF159706) is ~90% identical to hMunc13 (data not shown), suggesting that it represents a true rat ortholog of hMunc13. In addition, comparison with the known rat Munc13 sequences demonstrated that the novel protein is an N-terminal splice variant of rat Munc13-2 (Figures 1A and 1B). The novel N terminus contains 400 amino acid residues, including a core $C_2$ domain, and splices into the known rat Munc13-2 sequence at residue 764 of the published sequence, replacing an alternatively spliced N terminus of 763 residues (GenBank accession number U24071). Interestingly, a similar splicing event takes place in the *C. elegans* Munc13 homolog UNC-13, resulting in two variants with a common C-terminal region containing the $C_1$, $C_2$, and Munc13 homology domains and divergent N termini, one of which is homologous to that of Munc13-1 and the novel Munc13-2 splice variant described here (Eustance Kohn et al., 2000).

These data demonstrate that Munc13 genes consist of two modules that have evolved differentially and may have distinct functional roles. The C-terminal sequences starting with the $C_1$ domain and corresponding to the R region of *C. elegans* UNC-13 are highly conserved from *C. elegans* to human and present in all known UNC-13/Munc13 proteins. In contrast, the $C_2$ domain containing N terminus corresponding to the L region of *C. elegans* UNC-13 is only conserved in Munc13-1 and the novel N-terminal Munc13-2 splice variant (Figures 1B and 1C).

At the mRNA level, the novel splice variant of Munc13-2 is expressed in all tissues tested (heart, brain, spleen, lung, liver, skeletal muscle, kidney, and testis). Strongest signals in Northern blots labeled with a specific probe (bp 455–1088 of the novel sequence; GenBank accession number AF159706) at high stringency were obtained in lung and kidney (data not shown). Using a specific polyclonal antibody to the novel splice variant of Munc13-2, we determined its expression pattern at the protein level. The protein was detected in all tissues tested, with highest protein levels present in brain, lung, and testis (data not shown). This is in striking contrast to the previously published Munc13-2 splice variant, which is expressed only in brain (Brose et al., 1995; Augustin et al., 1999a). Therefore, we named the novel splice variant ubMunc13-2 (for "ubiquitously expressed") and the previously published "brain-specific" Munc13-2 splice variant bMunc13-2.

### The Conserved Munc13 N Terminus Defines a RIM1 Binding Domain

In the past, the search for UNC-13/Munc13 interaction partners concentrated on the conserved C-terminal regions of the proteins. The divergent N termini were largely neglected because of the apparent lack of evolutionary conservation. Proteins interacting with the UNC-13/Munc13 C terminus include Syntaxin, a core complex component with an essential role in exocytosis (Betz et al., 1997).

The presence of an evolutionary conserved N-terminal module in ubMunc13-2, Munc13-1, and *C. elegans* UNC-13LR suggests an as yet unrecognized common functional role for the N termini of these proteins. In order to identify proteins that interact with the ubMunc13-2 N terminus, we performed yeast two-hybrid screens using a rat brain cDNA prey library in pVP16-3 with the bait construct pLexN-ubMunc13-2(1-181), which en-

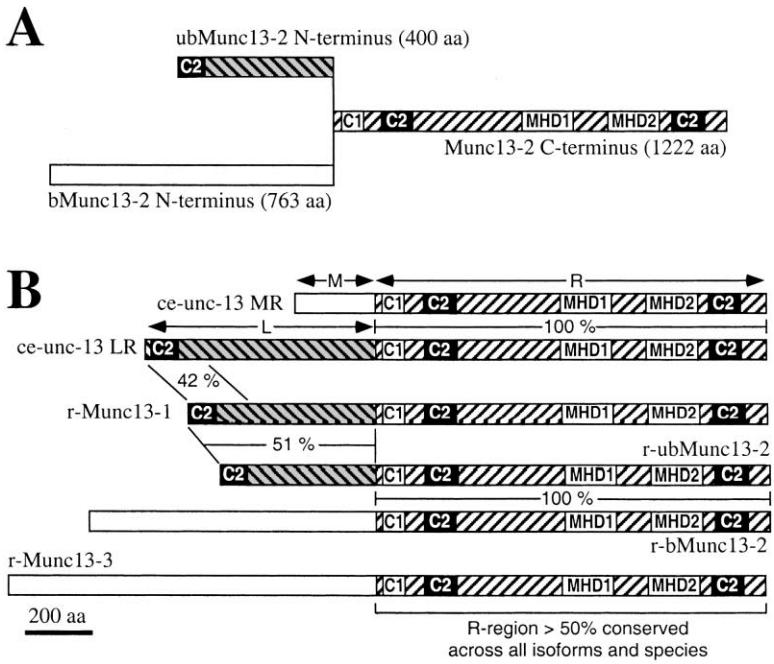


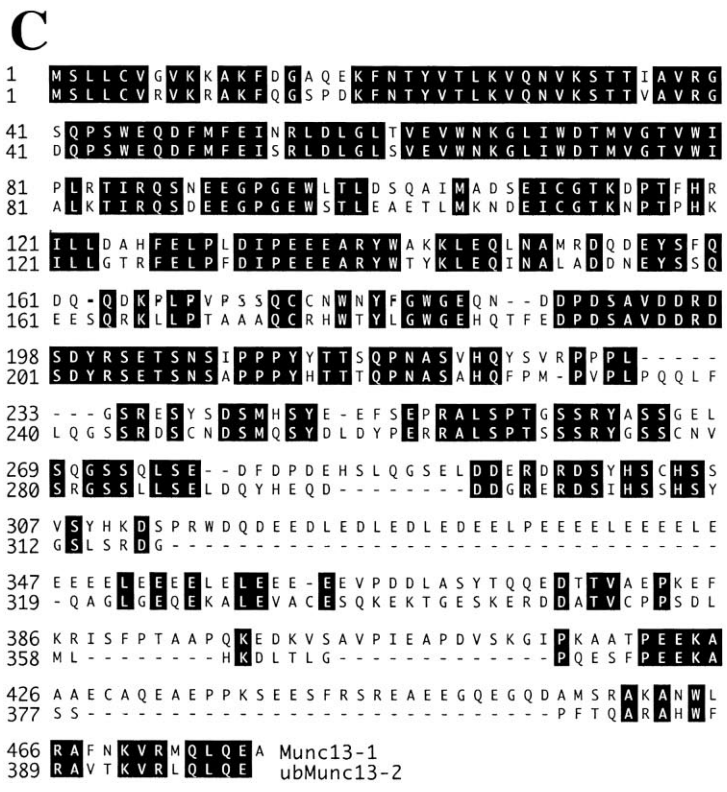


Figure 1. Differential Evolutionary Conservation of Protein Modules in the Munc13 Family

(A) Domain structures of Munc13-2 splice variants. bMunc13-2 and ubMunc13-2 differ in their alternatively spliced N termini. (B) Domain structure of UNC-13 homologs. Like rat Munc13-2, *C. elegans* UNC-13 (ce-unc-13) is expressed in two variants, MR and LR. The R region (black/white hatched) is highly conserved across all isoforms and species. The L region (black/gray hatched) is conserved in the rat homologs r-Munc13-1 and r-ubMunc13-2. All other UNC-13 homologs have completely unrelated N termini. The degree of identity between the different regions is given in percent. (C) Alignment of the conserved N termini of rat Munc13-1 and ubMunc13-2. Residues that are identical in the two sequences are shown on black background. C1, $C_1$ domain; C2, $C_2$ domain; ce, *C. elegans*; MHD, Munc13 homology domain; r, rat.

codes the first highly conserved 181 residues of ubMunc13-2 fused to LexA DNA binding domain (Figure 2A). We screened 90 million yeast transformants and isolated and sequenced a total of 80 positive prey clones. The sequenced clones contained a group of 11 partially overlapping prey vectors encoding the N-terminal Rab3 binding zinc finger region of the active zone protein RIM1 (Figure 2B): pPrey-RIM1(11-389) (residues 11–389 of RIM1, seven isolates), pPrey-RIM1(1-344) (residues 1–344 of RIM1, three isolates), and pPrey-RIM1(23-340) (residues 23–340 of RIM1 with a deletion of residues 177–180, one isolate). Apart from RIM1, no proteins with a putative or likely synaptic or active zone function were identified in our yeast two-hybrid screens.

Semiquantitative β-galactosidase assays demonstrated that the interaction is highly specific for the ubMunc13-2 N terminus, as pPrey-RIM1(1-344) interacted strongly with pLexN-ubMunc13-2(1-181) but not with

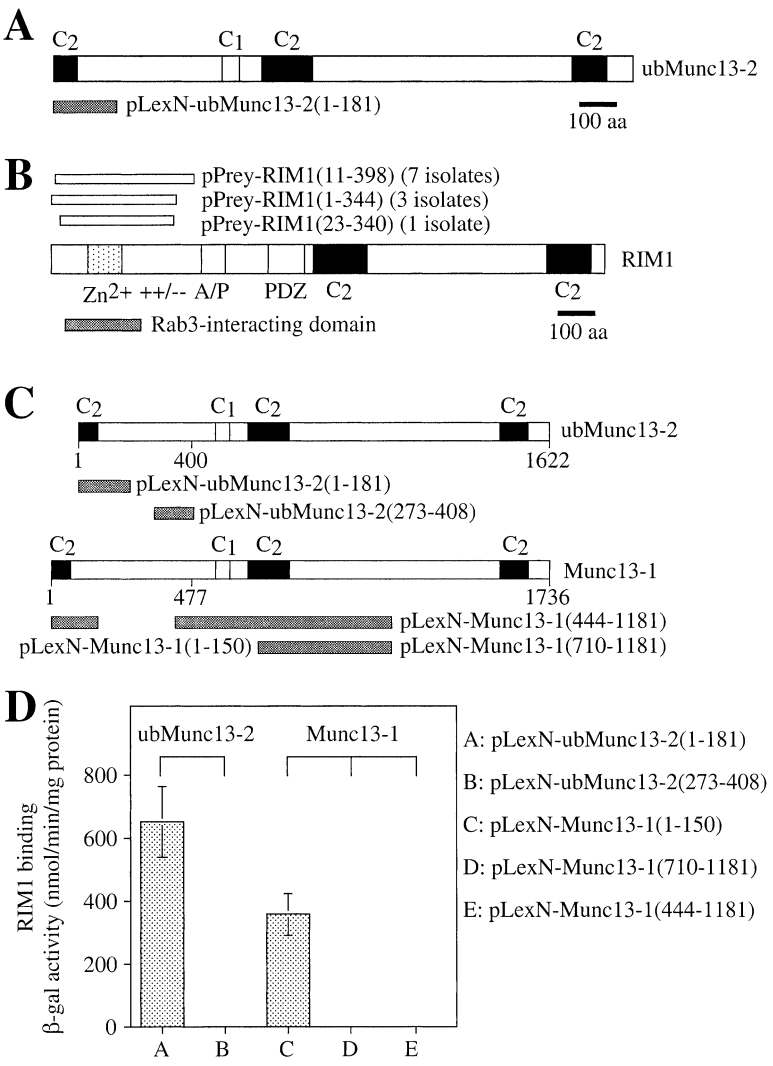


**Figure 2. The Conserved N Termini of Munc13-1 and ubMunc13-2 Bind RIM1 in the Yeast Two-Hybrid System**

(A) Domain structure of ubMunc13-2 and representation of the bait vector pLexN-ubMunc13-2(1-181) (gray bar) used in the yeast two-hybrid screen. (B) Domain structure of RIM1 and representation of the RIM1 prey clones (white bars) identified in yeast two-hybrid screens with pLexN-ubMunc13-2(1-181). The Rab3 interacting domain of RIM1 as identified by Wang et al. (1997) is shown as a gray bar. (C) Domain structures of ubMunc13-2 (top) and Munc13-1 (bottom) and representation of bait vectors used in semiquantitative yeast two-hybrid assays. (D) Semiquantitative analysis of interactions of ubMunc13-2 and Munc13-1 bait vectors with the RIM1 prey vector pPrey-RIM(1-344), using β-galactosidase assays. The N-terminal fragments of ubMunc13-2 and Munc13-1 interact strongly with RIM1, while respective control constructs do not. A/P, alanine/proline-rich sequence; $C_1$, $C_1$ domain; $C_2$, $C_2$ domain; PDZ, PDZ domain; $Zn^{2+}$, zinc finger; ++/−−, charged sequence.

the ubMunc13-2 control bait vector pLexN-ubMunc13-2(273-408) (Figures 2C and 2D). Given the homology between the ubMunc13-2 and Munc13-1 N termini, we next examined whether RIM1 also binds to Munc13-1. Like the ubMunc13-2 N terminus, a bait construct containing residues 1–150 of Munc13-1 [pLexN-Munc13-1(1-150)] interacted strongly with pPrey-RIM1(1-344), while a control construct [pLexN-Munc13-1(710-1181)] showed no interaction. Moreover, a bait construct containing the $C_2B$ domain of Munc13-1 [(pLexN-Munc13-1(444-1181)] did not interact with pPrey-RIM1(1-344). These data demonstrate that RIM1 binding is a common feature of the conserved N termini of Munc13-1 and ubMunc13-2 and is not caused by a $C_2$ domain–specific structural motif (Figures 2C and 2D).

To verify the yeast two-hybrid data with independent biochemical methods, we performed cosedimentation and immunoprecipitation assays with detergent extracts of synaptosomes. In a first set of cosedimentation assays, we used immobilized GST fusion proteins of Munc13-1 and ubMunc13-2 [GST-Munc13-1(3-317), GST-ubMunc13-2(2-320)] to precipitate RIM1 from detergent extracts. We found that both GST fusion proteins bound RIM1, while GST alone did not (Figure 3A, left). In addition, several other GST-Munc13-1 constructs [GST-Munc13-1(309-567), GST-Munc13-1(1032-1345), GST-Munc13-1(1399-1736)] did not bind to RIM1 in identical assays (Figures 3B and 3C). Again, these data demonstrate that RIM1 binding is a common characteristic of the Munc13-1 and ubMunc13-2 N termini. It is not caused by a $C_2$ domain-specific structural motif because the GST-Munc13-1(1399-1736) construct that contains the $C_2C$ domain of Munc13-1 does not bind to RIM1. For the following reasons, we concentrated in all following analyses on Munc13-1 whenever native Munc13 proteins were involved: (1) Munc13-1 is by far the most abundant Munc13 isoform in brain, its expression levels exceed that of ubMunc13-2 by at least one order of magnitude (data not shown), (2) Munc13-1 is the best-characterized Munc13 isoform for which the best detection tools are available (Brose et al., 1995; Betz et al., 1997, 1998; Augustin et al., 1999a), (3) Munc13-1 is the only Munc13 isoform that has been assigned a defined function in synaptic vesicle priming (Augustin et al., 1999b; Ashery et al., 2000), (4) Munc13-1 and RIM1 are colocalized at active zones (Wang et al., 1997; Betz et

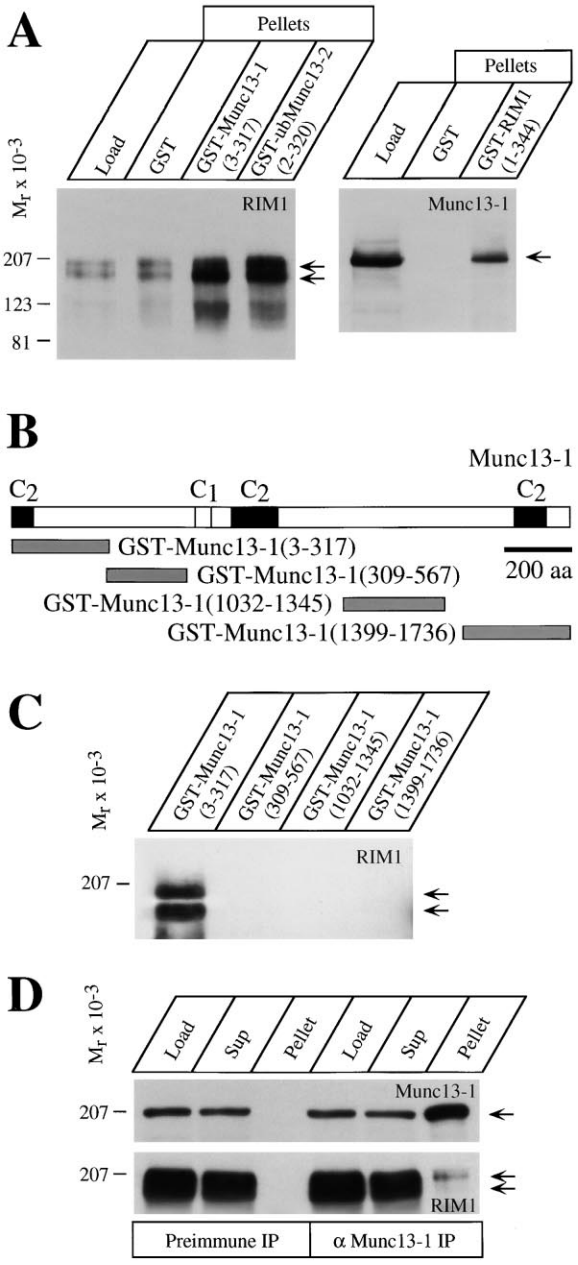


Figure 3. Munc13-1 and ubMunc13-2 Bind RIM1 in Cosedimentation and Immunoprecipitation Assays

(A) (Left) RIM1 binding to Munc13 GST fusion proteins in cosedimentation assays. Identical amounts of GST fusion proteins containing the N termini of Munc13-1 or ubMunc13-2 as well as GST alone were immobilized to glutathione agarose beads and used in cosedimentation assays with rat brain synaptosome extract. Proteins that bound to the immobilized GST fusion proteins were analyzed by SDS-PAGE and immunoblotting with antibodies specific to RIM1. Native RIM1 bound to both Munc13 fusion proteins but not to GST alone. (Right) Munc13-1 binding to RIM1-GST fusion proteins in cosedimentation assays. Identical amounts of GST or GST-RIM1(1-344) were used as described for left panel. Cosedimented proteins on blots were probed with antibodies specific to Munc13-1. Munc13-1 bound to the N-terminal RIM1 fusion protein but not to GST alone.

(B) Domain structure of Munc13-1 and representation of GST constructs used in the cosedimentation assays shown in (C). $C_1$, $C_1$ domain; $C_2$, $C_2$ domain.

(C) RIM1 binding to Munc13-1 GST fusion proteins in cosedimentation assays. Identical amounts of GST fusion proteins were used in cosedimentation assays as described for (A). Cosedimented proteins on blots were probed with antibodies specific to RIM1. Native RIM1 bound only to the fusion protein carrying the Munc13-1 N terminus.

(D) Coimmunoprecipitation of Munc13-1 and RIM1. Immunoprecipitation assays from rat brain synaptosome extract were done using a polyclonal antibody to Munc13-1 (αMunc13-1 IP) as well as the corresponding preimmune serum (Preimmune IP) as control. Identical amounts of the extract (Load), supernatant after immunoprecipitation (Sup), and immunoprecipitate (Pellet) were analyzed by SDS-PAGE and immunoblotting with antibodies specific to Munc13-1 (top) and RIM1 (bottom). RIM1 coimmunoprecipitates with Munc13-1.

al., 1998), and (5) studies in deletion mutant mice show that Munc13-1 is essential for survival (Augustin et al., 1999b), while ub/bMunc13-2 is not (N. B. and K. Reim, unpublished data). In the second type of cosedimentation assay, we used an immobilized GST fusion protein containing residues 1–344 of RIM1 [GST-RIM1(1-344)] to precipitate Munc13-1. As shown in Figure 3A (right), GST-RIM1(1-344) interacted strongly with Munc13-1, while GST alone did not. In a third set of experiments, we used a polyclonal antiserum to Munc13-1 in immunoprecipitation assays. Figure 3D shows that RIM1 coprecipitated with Munc13-1 in these experiments. Coprecipitation was specific because it was not observed in immunoprecipitates obtained with the corresponding preimmune serum. Together with RIM1, the core complex components Syntaxin, SNAP25, and VAMP/Synaptobrevin II coprecipitated with Munc13-1 in these experiments, while Rab3A did not (data not shown; see Betz et al., 1997, for corresponding data from Munc13-1 immunoprecipitations with the same antibody that was used here).

Taken together, our data demonstrate on the basis of three independent approaches (yeast two-hybrid, cosedimentation, and immunoprecipitation assays) that Munc13-1 and RIM1 interact physically. This conclusion is strongly supported by the fact that, in RIM1 deletion mutant mice, Munc13-1 levels in brain are reduced (T. C. Südhof, personal communication), which indicates that the half-life of Munc13-1 is reduced in the absence of its interaction partner RIM1.

### Munc13-1 and Rab3A Compete for the Same Binding Site in the RIM1 Zinc Finger Region

In order to map the respective interaction domains in Munc13-1, ubMunc13-2, and RIM1, we performed a series of yeast two-hybrid interaction tests and cosedimentation assays.

The N-terminal regions of Munc13-1 and ubMunc13-2 found to interact with RIM1 in yeast two-hybrid assays (residues 1–150 of Munc13-1 and residues 1–181 of ubMunc13-2) contain a highly degenerate core $C_2$ domain at their very N termini. To determine if this degenerated $C_2$ domain is responsible for RIM1 binding, we constructed bait vectors representing parts of the RIM1 binding regions of Munc13-1 and ubMunc13-2 [pLexN-Munc13-1(1-71), pLexN-Munc13-1(65-150), pLexN-ubMunc13-2(1-71), pLexN-ubMunc13-2(66-181)]. None

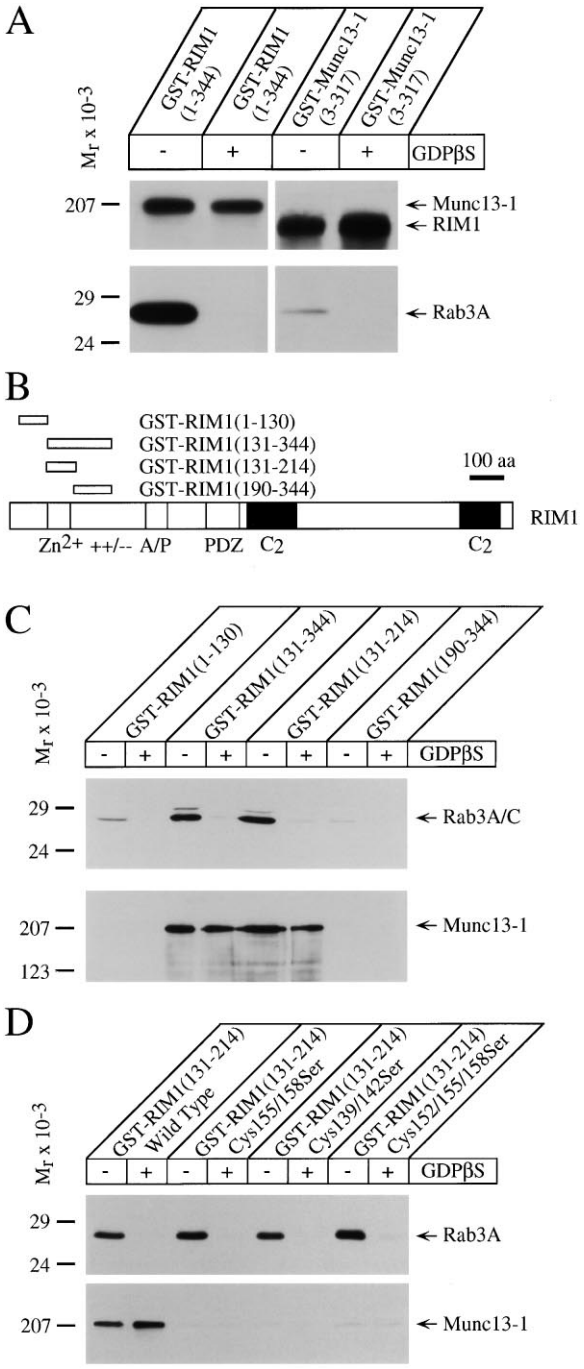


Figure 4. Munc13-1 and Rab3A Bind to the Same Zinc Finger Region in RIM1

(A) Munc13-1 and Rab3A binding to RIM1 is mutually exclusive. Identical amounts of N-terminal RIM1 and Munc13-1 fusion contructs with GST were used in cosedimentation assays as described for Figure 3A. To show the specificity of Rab3A binding, assays were performed in the absence (−) or presence (+) of GDPβS. Cosedimented proteins on blots were probed with antibodies specific to Munc13-1, RIM1, and Rab3A. RIM1 fusion protein bound both Munc13-1 and Rab3A (most likely due to the presence of two independent pools of RIM1 complexes in the assay [RIM1/Munc13-1 and RIM1/Rab3A]), while the Munc13-1 fusion protein only bound RIM1.

(B) Domain structure of RIM1 and representation of GST fusion constructs used in the mapping of the Munc13-1 binding site in RIM1. A/P, alanine/proline-rich sequence; $C_2$, $C_2$ domain; PDZ, PDZ domain; $Zn^{2+}$, zinc finger; ++/−−, charged sequence.

(C) Munc13-1 and Rab3A bind to the same 84 residue zinc finger domain of RIM1. The RIM1-GST fusion proteins depicted in (B) were used in cosedimentation assays as described for Figures 3A and 4A. Cosedimented proteins on blots were probed with antibodies specific to Munc13-1 and Rab3A/C. For binding of both Munc13-1 and Rab3A, an 84 residue zinc finger domain of RIM1 [GST-RIM1(131-214)] is sufficient.

(D) Mutation of cysteine residues in the RIM1 zinc finger abolishes binding of Munc13-1 but not of Rab3A. Identical amounts of GST fusion proteins with the minimal Munc13-1/Rab3A binding region of RIM1 (wild-type and indicated Cys to Ser mutations) were used for cosedimentaion assays as described for Figures 3A and 4A. Cosedimented proteins on blots were probed with antibodies specific to Munc13-1 and Rab3A. Mutations in the RIM1 zinc finger region abolish binding of Munc13-1 but not of Rab3A.

of these constructs were found to interact with RIM1 [pPrey-RIM1(1-344)], indicating that the first 150 residues of Munc13-1 and the first 181 residues of ubMunc13-2 form a functional RIM1 binding site, while the respective individual $C_2$ domains alone do not (data not shown). This finding further supports our above conclusion according to which RIM1 binding is not a general feature of $C_2$ domains (Figures 2D and 3C) but rather a characteristic of the whole conserved Munc13-1/ubMunc13-2 N-terminal region.

The N-terminal region of RIM1 (residues 1–344) that was found to interact with Munc13-1 and ubMunc13-2 in yeast two-hybrid interaction tests contains a zinc finger structure. Approximately the same region was previously shown to bind to Rab3A in a GTP-dependent manner (Wang et al., 1997). In order to determine whether Munc13-1 and Rab3A can bind to RIM1 simultaneously, we performed cosedimentation assays using immobilized GST fusion proteins of RIM1 [GST-RIM1(1-344)] and Munc13-1 [GST-Munc13-1(3-317)] in the absence or presence of GDPβS. As demonstrated in Figure 4A (left), GST-RIM1(1-344) bound Munc13-1 and Rab3A, the latter interaction being GTP dependent. In the reverse experiment, GST-Munc13-1(3-317) bound strongly to RIM1, while only background binding to Rab3A was observed (Figure 4A, right). These findings indicate that RIM1 cannot interact simultaneously with Munc13-1 and Rab3A and that the cosedimentation of Munc13-1 and Rab3A in experiments using immobilized GST-RIM1(1-344) is due to the presence of two independent pools of RIM1 complexes in the assay, RIM1/Munc13-1 and RIM1/Rab3A.

To examine the possibility that Munc13-1 and Rab3A indeed interact with the same region in the RIM1 N terminus, we mapped their respective binding sites in more detail. For that purpose, we generated a set of GST-RIM1 fusion proteins covering the entire interaction domain identified in the yeast two-hybrid experiments. Using these fusion proteins in cosedimentation assays, we mapped the binding sites of Munc13-1 and Rab3A to residues 131–214 of RIM1 [GST-RIM1(131-214)] (Figures 4B and 4C). Interestingly, a much weaker but GTP-dependent binding of Rab3A was also observed with GST-RIM1(1-130). This binding is likely to represent background binding of Rab3A [see also background Rab3A binding to GST-Munc13-1(3-317); Figure 4A].

However, we cannot exclude that an additional low-affinity Rab3A binding site resides in the very N terminus of RIM1.

In analogy to the Rab3 binding domain of another putative Rab3 effector, Rabphilin (Ostermeier and Brünger, 1999), the minimal Munc13-1/Rab3A binding region of RIM1 contains a zinc finger structure and short N- and C-terminal flanking regions. To determine the role of the RIM1 zinc finger in Munc13-1 and Rab3A binding, we generated mutant forms of the minimal binding region covered by GST-RIM1(131-214) in which two or three cysteine residues of the zinc finger were replaced by serines [GST-RIM1(131-214)Cys155/158Ser, GST-RIM1(131-214)Cys151/155/158Ser, and GST-RIM1 (131-214)Cys139/142Ser]. These mutants were then tested for Munc13-1 and Rab3A binding in cosedimentation assays. As shown in Figure 4D, all three mutations led to a complete loss of Munc13-1 binding. This finding provides an important additional indication of the specificity of the RIM1/Munc13-1 interaction. In contrast to Munc13-1, Rab3A binding was not affected by the mutations in the RIM1 zinc finger (Figure 4D), although similar mutations in the Rabphilin zinc finger abolish Rab3 binding (Stahl et al., 1996). This demonstrates that the Rab3 binding regions in RIM1 and Rabphilin are differentially affected by the zinc finger structure and suggests differences between Rabphilin and RIM with respect to the mechanism of Rab3 binding.

As the Munc13-1 and Rab3 binding sites in RIM1 mapped to the same RIM1 sequence (residues 131–214), we examined in subsequent experiments if Munc13-1 and Rab3A compete for the same binding site in RIM1. For that purpose, we performed cosedimentation assays using immobilized GST-RIM1(131-214). As demonstrated in Figure 5, binding of native Rab3A and Munc13-1 from synaptosomal detergent extracts was progressively inhibited in the presence of increasing concentrations of a recombinant RIM1 binding Munc13-1 fragment [Munc13-1(3-317)] whose GST tag had been cleaved off. The progressive inhibition of binding of native Rab3A and Munc13-1 was paralleled by a concentration-dependent increase in the binding of competitor. The half-maximal effective concentration of the competitor fragment Munc13-1(3-317) was 250 nM for displacement of Rab3A and 500 nM for displacement of Munc13-1. The actual affinity of the competitor for RIM1 may be higher because the amount of correctly folded protein most likely represents only a fraction of the total protein used in the assay. Because Rab3A does not bind directly to Munc13-1 (Figure 4A; see also Betz et al., 1997), these data demonstrate that binding of Munc13-1 and Rab3A to RIM1 is competitive and mutually exclusive.

### Binding of RIM1 and Synaptic Vesicle Priming Are Mediated by Distinct Modules of Munc13-1

The independent evolutionary conservation of the N-terminal L region of Munc13-1/ubMunc13-2 and the C-terminal R region is indicative of distinct and partially independent roles of these protein modules in active zone function. We showed previously that the R regions of Munc13-1, -2, and -3 contain functional Syntaxin binding domains (Betz et al., 1997; Augustin et al., 1999a) and speculated that Syntaxin binding by the Munc13-1

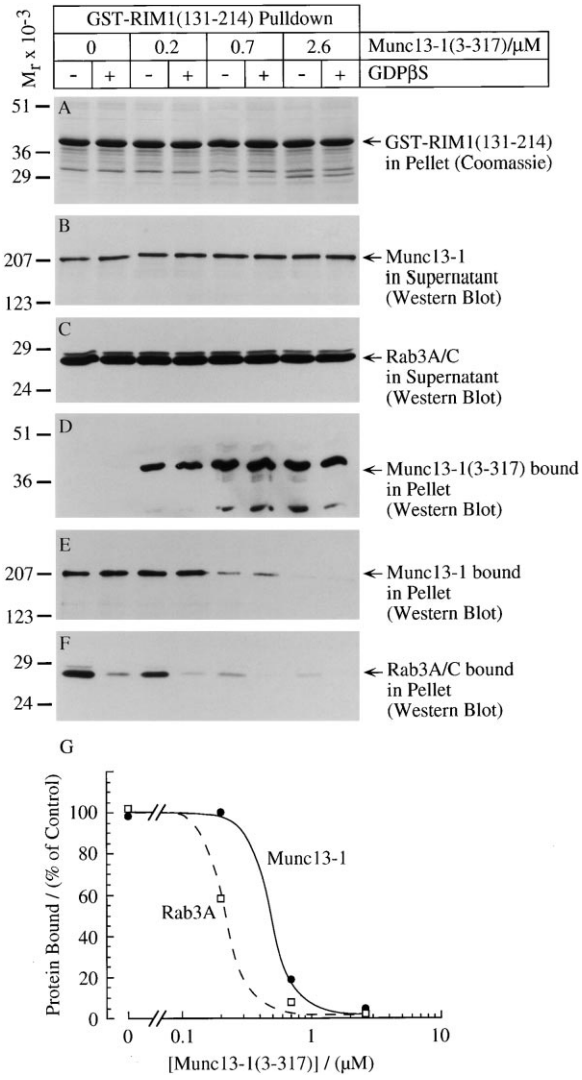


Figure 5. Binding of Munc13-1 and Rab3A to the RIM1 Zinc Finger Region Is Competitive

Identical amounts of GST fusion proteins with the minimal Munc13-1/Rab3A binding region of RIM1 [GST-RIM1(131-214)] were immobilized on glutathione agarose and used in cosedimentation assays with rat brain synaptosome extract. Assays were performed in the presence of increasing concentrations of a recombinant Munc13-1 competitor fragment that represents the RIM1 binding region of Munc13-1 [Munc13-1(3-317)]. For each concentration of the competitor, assays were performed in the absence (−) or presence (+) of GDPβS. To verify that no degradation of proteins had taken place during the assay, the amounts of GST-RIM1(131-214) in the pellet (A) and of excess native Munc13-1 and Rab3A/C in the supernatant after the cosedimentation assay (B and C) were determined. Proteins that bound to the immobilized GST-RIM1(131-214) fusion proteins were analyzed by SDS-PAGE and immunoblotting with antibodies specific to Munc13-1 and Rab3A/C. The amount of the recombinant competitor Munc13-1(3-317) bound to the immobilized RIM1 fusion protein increased with increasing competitor concentrations (D). The increased binding of competitor led to a concomitant displacement of bound native Munc13-1 and Rab3A/C (E and F), demonstrating that Munc13-1 and Rab3A compete for the same binding site in RIM1. (G) A quantitative densitometric analysis of bands shown in (E) and (F).

R region is of central importance for the priming activity of Munc13-1 (Brose et al., 2000). On the other hand, the present data suggest that the N-terminal L region of Munc13-1 is involved in a partially independent, active zone–specific function of Munc13-1 by mediating the interaction with the active zone protein RIM1.

To test directly whether the C-terminal R region of Munc13-1 can function as an independent priming module, we examined the effects of overexpression of various Munc13-1EGFP constructs on $Ca^{2+}$-dependent secretion from bovine chromaffin cells. In these cells, a rapid increase in intracellular $Ca^{2+}$ by flash photolysis of caged $Ca^{2+}$ leads to an exocytotic burst, which reflects release of chromaffin granules from readily releasable pools, followed by a sustained phase of secretion, which reflects vesicle priming and subsequent fusion during ongoing stimulation. Both burst and sustained phases of secretion can be assessed with high time resolution membrane capacitance measurements (Neher, 1998).

Chromaffin cells were held in the whole-cell mode to allow both dialysis of the $Ca^{2+}$ cage nitrophenyl-EGTA into the cytoplasm and membrane capacitance measurements (Ashery et al., 2000). We showed previously that overexpression of a full-length Munc13-1EGFP fusion protein [Munc13-1(1-1736)EGFP] in chromaffin cells using the Semliki Forest virus system leads to a massive increase in chromaffin granule priming rates, resulting in a 3-fold amplitude increase of the burst and sustained phases of secretion compared to control cells (Figure 6; Ashery et al., 2000). Interestingly, overexpression of Munc13-1 constructs lacking either the RIM1 binding region [Munc13-1(162-1736)EGFP] or the entire N-terminal L region [Munc13-1(520-1736)EGFP] also caused increases in $Ca^{2+}$-triggered secretion that were very similar to those observed for the full-length construct Munc13-1(1-1736)EGFP (Figure 6). In contrast, overexpression of the RIM1 binding N terminus of Munc13-1 [Munc13-1(1-451)EGFP] alone had no effect, although the construct was expressed at high levels as assessed by EGFP fluorescence (Figure 6). Corresponding values for the burst and sustained components of release were as follows: 238 ± 32 fF (n = 13) and 123 ± 62 fF (n = 13) for uninfected control cells in the experiments with full-length and C-terminal fragments of Munc13-1 with priming activity (averaged trace not shown in Figure 6); 339 ± 41 fF (n = 9) and 67 ± 20 fF (n = 9) for uninfected control cells in the experiment with the N-terminal RIM1 binding Munc13-1 fragment (averaged control trace in Figure 6); 1485 ± 227 fF (n = 17) and 630 ± 144 fF (n = 17) for cells overexpressing Munc13-1(1-1736)EGFP; 1269 ± 285 fF (n = 12) and 731 ± 205 fF (n = 12) for cells overexpressing Munc13-1(162-1736)EGFP; 1669 ± 311 fF (n = 10), 804 ± 172 fF (n = 10) for cells overexpressing Munc13-1(520-1736)EGFP; 279 ± 45 (n = 9) and 101 ± 20 (n = 9) for cells overexpressing Munc13-1(1-451)EGFP. For all tested constructs except Munc13-1(1-451)EGFP, secretion in overexpressing cells was significantly increased compared to control cells ($p < 0.01$–$0.002$). No statistical differences between the three active constructs were observed. Data obtained with the N-terminal fragment Munc13-1(1-451)EGFP were not significantly different from control data. These experiments demonstrate that the C-terminal R region of Munc13-1 is a partially independent vesicle priming module and does not need a RIM1 binding region for its priming function in chromaffin cells. On the other hand, the RIM1 binding region alone has no effect on secretion from chromaffin cells.

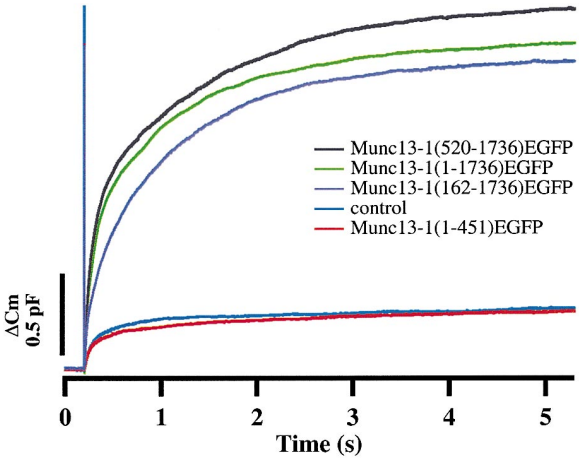


Figure 6. Munc13-1-Mediated Priming of Chromaffin Granules Is Independent of the RIM1 Binding Region

Averaged high time resolution recordings of membrane capacitance changes in chromaffin cells in response to flash photolysis (vertical line) of caged $Ca^{2+}$ (~20 μM free $Ca^{2+}$ after flash; data not shown). Semliki Forest virus–mediated overexpression of EGFP-tagged full-length Munc13-1 [Munc13-1(1-1736)EGFP, green, n = 17] as well as of EGFP-tagged, N-terminally truncated, RIM binding-deficient constructs [Munc13-1(162-1736)EGFP, purple, n = 12; Munc13-1(520-1736) EGFP, black, n = 10] leads to a strong increase in burst and sustained phases of secretion that was significantly higher ($p < 0.01$–$0.002$) than that observed in control cells (n = 13, control trace not shown but similar to the one shown). No significant differences between the three secretion-enhancing constructs were observed. Secretion from chromaffin cells overexpressing the RIM binding N-terminal fragment of Munc13-1 [Munc13-1(1-451)EGFP, red, n = 9] was indistinguishable from that observed in control cells from the same cultures (control, blue, n = 9).

### Perturbation of Munc13-1/RIM1 Interaction In Vivo Leads to a Reduction in the Number of Readily Releasable Vesicles

In order to investigate the physiological role of the Munc13-1/RIM1 interaction in vivo, we studied the effects of Semliki Forest virus–mediated overexpression of various Munc13-1EGFP fusion constructs in mouse hippocampal neurons in culture. In a first set of experiments, we overexpressed the RIM1 binding region of Munc13-1 [Munc13-1(1-451)EGFP] in wild-type neurons. We expected that this construct would act in a dominant-negative manner, as it binds RIM1 but is priming deficient because it lacks the R region that is responsible for the priming function (see Figure 6). In addition to this putative dominant-negative construct, we studied the effects of overexpression of full-length Munc13-1 [Munc13-1(1-1736)EGFP] and of a RIM1 binding-deficient, priming-competent Munc13-1 construct [Munc13-1(520-1736)EGFP] in wild-type neurons. Only glutamatergic neurons were included in the analysis because priming of vesicles by Munc13-1 is specific for glutamatergic synapses in hippocampal primary neurons (Augustin et al., 1999b).

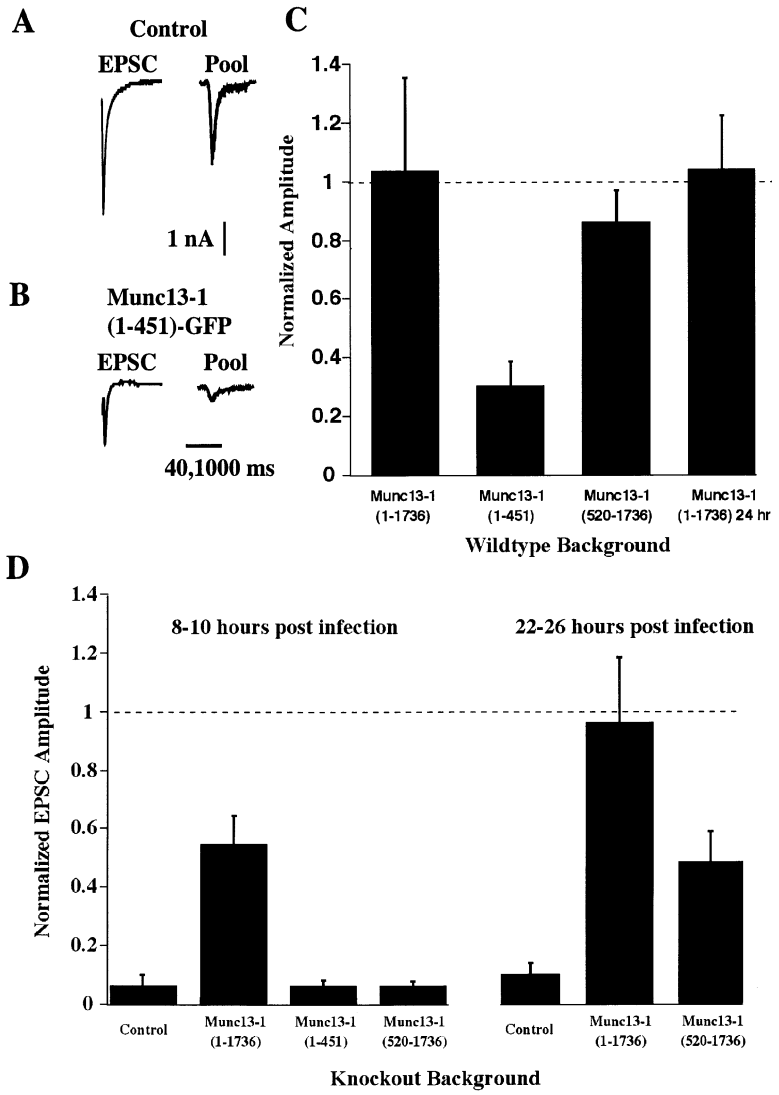


Figure 7. Dominant-Negative and Rescue Activities of Munc13-1 Constructs in Wild-Type and Munc13-1 Knockout Neurons

(A and B) (Left) AMPA receptor–mediated EPSCs from a wild-type control neuron (A) and a wild-type neuron overexpressing Munc13-1(1-451)EGFP (B). (Right) Vesicle pool measurements by application of hypertonic sucrose solution (500 mM sucrose added to the external medium at onset of signal) to the entire dendritic tree of a wild-type control neuron (A) and a wild-type neuron overexpressing Munc13-1(1-451)EGFP (B). Note the parallel reduction of EPSC amplitudes and sucrose responses following overexpression of Munc13-1(1-451)EGFP. Horizontal bar indicates 40 ms for EPSC recordings and 1000 ms for pool recordings.

(C) Summary histogram of average evoked synaptic peak current amplitudes obtained in wild-type neurons overexpressing the indicated constructs (8–10 hr postinfection; 24 hr postinfection for right bar). Data were normalized to the respective wild-type control values measured in uninfected cells from the same cultures at the same days. Values of n are (from left to right) 8, 15, 39, and 16. Note that overexpression of Munc13-1(1-451)EGFP leads to a significant reduction in EPSC amplitudes as compared to wild-type control cells ($p < 0.001$). In contrast, the other tested constructs have no effect.

(D) Summary histogram of average evoked synaptic peak current amplitudes obtained in Munc13-1 knockout neurons overexpressing the indicated constructs. Left panel, 8–10 hr postinfection; right panel, 22–26 hr postinfection. Data from Munc13-1 knockout cultures were normalized to the respective values measured at the same days in wild-type sister cultures that were obtained from wild-type littermates. Values of n are (from left to right) 26, 28, 9, 10, 6, 18, and 5. Note that overexpression of full-length Munc13-1(1-1736)EGFP at 8–10 hr postinfection significantly rescues the Munc13-1 knockout phenotype ($p < 0.01$ compared to Munc13-1 knockout control), while the RIM1 binding-deficient construct Munc13-1(520-1736)EGFP and the priming-deficient construct Munc13-1(1-451)EGFP do not. At 22–26 hr postinfection, full-length Munc13-1(1-1736)EGFP reconstitutes a wild-type phenotype ($p < 0.001$), and the RIM1 binding-deficient Munc13-1(520-1736)EGFP construct induces a partial but significant rescue ($p < 0.05$).

As shown in Figures 7A–7C, overexpression of Munc13-1(1-451)EGFP for 8–10 hr postinfection led to a dramatic reduction of excitatory postsynaptic responses upon action potential–evoked release from mouse wild-type neurons. Excitatory postsynaptic currents (EPSCs) were 3.84 ± 0.56 nA ($n = 15$) in control cells and 1.16 ± 0.26 nA ($n = 15$) in overexpressing cells ($p < 0.001$). In contrast, overexpression of full-length Munc13-1 [Munc13-1(1-1736)EGFP] for 8–26 hr postinfection and of the N-terminally truncated, RIM1 binding-deficient form Munc13-1(520-1736)EGFP for 8–10 hr postinfection had no effect, although they were expressed at high levels as assessed by EGFP fluorescence. Corresponding EPSC values for uninfected control cells and infected cells (measured from the same cultures on the same day) were as follows: 4.08 ± 1.3 nA ($n = 8$) and 4.26 ± 0.84 nA ($n = 8$, $p > 0.5$) for Munc13-1(1-1736)EGFP at 8–10 hr postinfection; 2.25 ± 0.28 nA ($n = 39$) and 1.93 ± 0.24 nA ($n = 39$, $p > 0.5$) for Munc13-1(520-1736)EGFP at 8–10 hr postinfection; and 1.80 ± 0.33 nA ($n = 16$) and 1.72 ± 0.43 nA ($n = 16$, $p > 0.5$) for Munc13-1(1-1736)EGFP at 24 hr postinfection. EPSC measurements are summarized in Figure 7C, in which, due to the variability of absolute EPSC amplitudes between cultures from different experiments/days, values are normalized to those of the respective wild-type controls. These data demonstrate that Munc13-1(1-451)EGFP indeed acts in a dominant-negative manner and causes a decrease in neurotransmitter release upon overexpression in wild-type neurons.

Munc13-1-deficient neurons are characterized by a drastically reduced pool of readily releasable vesicles (Augustin et al., 1999b). In order to determine if the reduction of EPSCs we observed in Munc13-1(1-451)EGFP-overexpressing neurons (Figures 7A–7C) is due to an underlying reduction in the size of the readily

releasable vesicle pool, we assayed the size of this pool by application of hypertonic sucrose solution. As in the case of synaptically evoked responses, we found that excitatory postsynaptic responses induced by application of hypertonic sucrose solution were markedly reduced in wild-type rat hippocampal neurons overexpressing Munc13-1(1-451)EGFP. The degree of this reduction was comparable to that observed for synaptically evoked responses (total charge transfer 0.68 ± 0.1 nC, n = 16, in control cells; 0.20 ± 0.04 nC, n = 11, in overexpressing cells, $p < 0.001$; sample traces in Figures 7A and 7B). The ratio between total charge transfer during an EPSC and that during sucrose stimulation was not significantly altered when overexpressing cells were compared to wild-type control cells. This suggests that vesicular release probability is not altered by the Munc13-1(1-451)EGFP overexpression and that the observed reduction in EPSC amplitude is indeed due to an underlying reduction in the size of the readily releasable vesicle pool. Thus, overexpression of Munc13-1(1-451)EGFP in wild-type neurons creates a phenocopy of Munc13-1-deficient nerve cells.

### Compromised Function of a RIM1 Binding-Deficient Munc13-1 Construct in Neurons

In complementary experiments, the effects of Munc13-1EGFP constructs were studied in the Munc13-1 deletion mutant background. As shown in Figure 7D, overexpression of full-length Munc13-1 [Munc13-1(1-1736)EGFP] in Munc13-1-deficient cells led to a significant increase of EPSCs as compared to uninfected Munc13-1 knockout cells at 8–10 hr postinfection. EPSC values were 0.20 ± 0.066 nA (n = 26) for knockout control cells and 1.97 ± 0.56 nA (n = 28, $p < 0.01$) in knockout cells overexpressing full-length Munc13-1(1-1736)EGFP. While Munc13-1-deficient neurons show evoked responses that amount to about 5%–10% of their respective wild-type control cells in "sister" cultures, values measured in the overexpressing cells approached 60% of those observed in wild-type control cells (Figure 7D), demonstrating that the Munc13-1 deletion mutant phenotype can be rescued by overexpression of full-length Munc13-1. In contrast, overexpression of the RIM1 binding region of Munc13-1 alone [Munc13-1(1-451)EGFP] or of a RIM1 binding-deficient but priming-competent form of Munc13-1 [Munc13-1(520-1736)EGFP] had no effect on EPSC amplitudes in Munc13-1-deficient neurons despite high levels of expression as assessed by EGFP fluorescence. Corresponding EPSC amplitudes in naive and infected Munc13-1 knockout neurons were as follows: 0.081 ± 0.026 nA (n = 10) and 0.082 ± 0.034 nA (n = 9, $p > 0.5$) for Munc13-1(1-451)EGFP, and 0.114 ± 0.017 nA (n = 26) and 0.121 ± 0.028 nA (n = 10, $p > 0.5$) for Munc13-1(520-1736)EGFP. A summary of these data is shown in Figure 7D (left). In order to correct for the variability in absolute EPSC amplitudes between cultures from different experiments/days, values were normalized to those measured at the same days in corresponding wild-type sister cultures. These data demonstrate that the changes observed in mouse wild-type neurons overexpressing the dominant-negative Munc13-1(1-451)EGFP construct (see Figure 7C) are not caused by nonspecific or toxic effects of the overexpressed protein but rather likely due to an interference with a Munc13-1-specific reaction. Moreover, these data show that, in contrast to full-length Munc13-1, priming-deficient [Munc13-1(1-451)EGFP] or RIM1 binding-deficient forms of Munc13-1 [Munc13-1(520-1736)EGFP] cannot rescue the Munc13-1 knockout phenotype 8–10 hr postinfection. Thus, in contrast to chromaffin cells (Figure 6), both the RIM1 binding N terminus as well as the R region of Munc13-1 that carries the priming activity are necessary for proper function in neurons.

Interestingly, the RIM1 binding-deficient form of Munc13-1 [Munc13-1(520-1736)] [but not the priming-deficient Munc13-1(1-451)EGFP; data not shown] did lead to a significant rescue (50% of wild-type control values in sister cultures) of the Munc13-1 knockout phenotype when cells were analyzed at 22–26 hr postinfection (Figure 7D, right). Under the same conditions, overexpression of full-length Munc13-1(1-1736)EGFP completely reconstituted a wild-type phenotype in knockout cells (95% of wild-type EPSC values measured in sister cultures). Corresponding EPSC values in naive and infected Munc13-1 knockout cells were as follows: 0.128 ± 0.041 nA (n = 6) and 1.314 ± 0.312 nA (n = 18, $p < 0.001$) for Munc13-1(1-1736)EGFP, and 0.09 ± 0.03 nA (n = 6) and 0.451 ± 0.093 nA (n = 5, $p < 0.05$) for Munc13-1(520-1736)EGFP. These values were normalized to the respective wild-type control values measured in wild-type sister cultures at the same days and are summarized in Figure 7D (right).

From biochemical data on Semliki Forest virus–mediated overexpression of proteins in various cell types, we estimated that 22–26 hr postinfection levels of overexpressed Munc13-1 protein are increased 40- to 100-fold in comparison to wild-type levels (Ashery et al., 2000). In the case of neurons, we found that overexpressed EGFP fusion proteins essentially flooded the cells including processes and presynaptic terminals (data not shown). Taken together, our data on the postinfection time course of effects caused by overexpression of Munc13-1(520-1736)EGFP in Munc13-1 knockout neurons (no effect at 8–10 hr in contrast to significant rescue by full-length Munc13-1; partial rescue at 22–26 hr postinfection in contrast to complete rescue by full-length Munc13-1) demonstrate that the RIM1 binding-deficient Munc13-1(520-1736)EGFP is clearly dysfunctional in neurons. However, once expression levels of Munc13-1(520-1736)EGFP in neurons reach extremely high levels, flooding neuronal processes and presynaptic terminals, it can function as a priming protein in presynaptic terminals, albeit with a significantly lower efficiency than full-length Munc13-1.

## Discussion

### Differential Evolution of RIM Binding and Priming Modules in Munc13 Proteins

The primary structures of the three originally identified mammalian UNC-13 homologs (Munc13-1, bMunc13-2, and Munc13-3; Brose et al., 1995; Augustin et al., 1999a) and of the corresponding *C. elegans* and *Drosophila* proteins are very similar in their C-terminal regions, including regulatory $C_1$ and $C_2$ domains as well as Munc homology domains (Figure 1B; Koch et al., 2000). This

indicates a high degree of evolutionary and functional conservation in this region. In contrast, the N-terminal regions of UNC-13-like proteins are only conserved in certain isoforms or splice variants and are otherwise completely unrelated. In *C. elegans*, N-terminal alternative splicing generates two variants of UNC-13, MR and LR (Figure 1B; Eustance Kohn et al., 2000). One of these (LR) contains an N terminus that is highly homologous to that of Munc13-1, while the other variant has a shorter, completely unrelated N-terminal sequence (Figure 1B). We now show that a similar splicing event at a similar site occurs in Munc13-2 transcripts, generating a ubiquitously expressed variant, ubMunc13-2, with an N-terminal sequence that is similar to that of UNC-13LR and Munc13-1, and a brain-specific variant, bMunc13-2, with a completely unrelated N terminus (Figures 1A–1C). Taken together, these data suggest that UNC-13-like proteins are built from two functional modules that have evolved differentially: (1) a C-terminal part, corresponding to the R region in UNC-13, that is highly conserved through evolution and present in all bona fide members of the UNC-13 family; and (2) an N-terminal part that is only conserved in certain isoforms or splice variants, while other isoforms or splice variants have completely divergent N termini that represent later evolutionary acquisitions.

The differentially evolved Munc13 modules have distinct functional roles in Munc13-1. The generally conserved C-terminal R region, which contains the interaction sites for most putative UNC-13/Munc13 effectors (Syntaxin, DOC2$\alpha$, $\beta$-spIII$\Sigma$, msec7-1; Brose et al., 2000), is necessary and sufficient for optimal secretory vesicle priming in chromaffin cells (Figure 6). The N-terminal RIM binding L region of Munc13-1, on the other hand, appears to convey a synapse-specific function that is not directly involved in the priming reaction but appears to influence it indirectly. Disruption of the RIM1/Munc13-1 interaction in wild-type neurons results in a deficiency in synaptic vesicle priming that is reminiscent of the Munc13-1 knockout phenotype (Figure 7). This finding suggests that RIM binding to Munc13-1 has an important regulatory function in the presynapse (e.g., by anchoring Munc13-1 in the active zone and thereby positioning it for optimal function or by modulating the priming and secretion apparatus [see below]). This is further supported by the finding that RIM binding-deficient Munc13-1 is functionally compromised in neurons, as it is not able to completely rescue the Munc13-1 knockout phenotype upon overexpression (Figure 7).

The view that the N-terminal RIM binding L region of Munc13-1 conveys a synapse-specific function is supported by studies in *C. elegans*. Here, the UNC-13LR form, which is entirely homologous to Munc13-1 and contains both a putative RIM binding domain in its L region as well as the highly conserved R region that harbors the priming activity, is mainly localized to the presynapse. In contrast, the UNC-13MR form exhibits a more diffuse distribution. However, UNC-13MR is also present in synapses, suggesting the existence of multiple synaptic targeting sequences in UNC-13 proteins (Eustance Kohn et al., 2000). An additional parallel between the present study and data from *C. elegans* is apparent with respect to the rescue ability of different UNC-13/Munc13-1 constructs in the *unc-13*/Munc13-1 null mutant background. We show here that a RIM binding-deficient Munc13-1 construct lacking the L region is dysfunctional and only able to partially rescue the Munc13-1 deletion mutant phenotype even upon very strong overexpression. In contrast, full-length Munc13-1 completely rescues the Munc13-1 knockout phenotype (Figure 7). Similarly, transgenic rescue of *C. elegans unc-13* null alleles using a cosmid that is only able to replace the RIM binding-deficient UNC-13MR is incomplete, as determined on the basis of behavioral parameters, while rescue with a cosmid that also replaces the RIM binding UNC-13LR form is much more effective (Eustance Kohn et al., 2000).

### Munc13-1/RIM1 Interaction: Functional Consequences and Their Molecular Mechanism

Two striking characteristics of neurotransmitter release at the synapse are its spatial restriction to active zones and its efficiency even at very high action potential frequencies. These characteristics suggest that vesicle trafficking steps at the active zone are occurring in a spatially and temporally coordinated manner. In order to guarantee such spatial and temporal coordination, the main active zone processes of vesicle tethering, priming, and fusion are likely to be coupled at the molecular level. The most efficient way to achieve molecular coupling between active zone–specific reactions would be a direct interaction of proteins that mediate consecutive steps in active zone function.

Munc13-1 is an essential component of the synaptic vesicle priming process in active zone function. It is thought to promote vesicle priming by modifying the conformation of the core complex component Syntaxin, thereby regulating the availability of Syntaxin for core complex formation (Augustin et al., 1999b; Ashery et al., 2000; Brose et al., 2000). RIM1, on the other hand, was originally identified as a putative Rab3 effector in the active zone (Wang et al., 1997). Its role is therefore likely to be at least partially linked to that of Rab3 proteins. Suggested functions of Rab proteins and their effectors include roles in vectorial vesicle transport, vesicle tethering, core complex assembly, and regulation of a very late step in synaptic vesicle exocytosis by limiting the number of vesicles that are released during an action potential (Fernandez-Chacon and Südhof, 1999; Gonzalez and Scheller, 1999).

The present data demonstrate that the Munc13-1/RIM interaction is essential for a step in the synaptic vesicle cycle that precedes vesicle fusion. Similar to total loss of Munc13-1, disruption of this interaction in wild-type hippocampal neurons leads to a drastically reduced primed and readily releasable vesicle pool, which in turn causes a strong reduction in evoked release. Regulation of the size of the readily releasable vesicle pool by the Munc13-1/RIM1 interaction may be mediated by at least three different mechanisms, all of which are in accord with the present data, in that they predict that disruption of the Munc13-1/RIM1 interaction would severely affect vesicle priming, leading to a reduction of the readily releasable vesicle pool.

First, RIM may simply serve to target Munc13-1 to the presynapse. Disruption of the interaction would lead to

reduced presynaptic concentrations of Munc13-1 and compromised vesicle priming. For a number of reasons, this scenario is unlikely. In our overexpression studies, we found no evidence of striking differences between full-length Munc13-1(1-1736)EGFP, the RIM binding-deficient Munc13-1(520-1736)EGFP, and the priming-deficient Munc13-1(1-451)EGFP with respect to synaptic targeting (data not shown). This suggests that Munc13-1 contains at least two different presynaptic targeting sequences, only one of which may be related to the RIM binding site. Indeed, Munc13-3, which contains no RIM binding sequence but is otherwise highly homologous to Munc13-1, exhibits a presynaptic localization in cerebellum that is indistinguishable from that of Munc13-1 (Augustin et al., 1999a), further demonstrating that RIM binding by Munc13s is not essential for their presynaptic targeting. Biochemical experiments show that disruption of the RIM1/Munc13-1 interaction in isolated active zone/postsynaptic density (PSD) preparations by addition of a soluble, RIM binding Munc13-1 fragment [Munc13-1(3-317), as used in Figure 5] does not displace Munc13-1 from active zones/PSDs, while limited protease treatment with Thrombin leads to release of full-length Munc13-1 (H. J. J. and N. B., unpublished data). This suggests that a protein other than RIM anchors Munc13-1 at active zones.

Second, RIM may contribute to vesicle tethering by binding to Rab3A and create a physical link between the tethering and priming apparatus by interacting with Munc13-1. According to this model, Rab3A-GTP on the synaptic vesicle binds to RIM1 on the active zone membrane upon synaptic vesicle tethering to the active zone. Next, the N terminus of Munc13-1 binds to RIM1. This step links the tethering and priming apparatus in the microenvironment of the active zone. Upon RIM1 binding, Munc13-1 displaces Rab3A, which may dissociate from the vesicle surface after GTP hydrolysis. Rab3A displacement and RIM1 binding by Munc13-1 then initiate core complex assembly to which GTP hydrolysis by Rab3A may further contribute. It is possible that, upon binding to RIM1, Munc13-1 is already associated with a Syntaxin/SNAP25 dimer. This model implies that a tight colocalization of RIM1 and Munc13-1 in the microenvironment of the active zone is essential for optimal vesicle priming and suggests that Munc13-1 acts as a physical bifunctional linker between vesicle tethering and priming.

Third, RIM binding to the Munc13-1 N terminus may directly regulate the priming activity of Munc13-1. Munc13-1 is essential for synaptic vesicle priming (Augustin et al., 1999b), and vesicle priming is likely to be the rate-limiting step in many secretory processes, including catecholamine release from chromaffin cells (Ashery et al., 2000). Thus, modulation of the activity of the Munc13-1 pool in the active zone by protein interactors such as RIM1 (see above) or by second messengers such as diacylglycerol (Betz et al., 1998) is a likely mechanism that dynamically regulates the pool of readily releasable vesicles and synaptic efficacy. In contrast, the overall cellular concentration of Munc13-1 in wild-type neurons appears to be much less critical, as overexpression of full-length Munc13-1(1-1736)EGFP does not increase transmitter release (Figure 7C). In view of the present data, it is tempting to speculate that the functions of RIM are mediated via Munc13-1 as the main "output" molecule with core complex formation and vesicle priming as the target processes. Our data suggest that RIM1 signaling to Munc13-1 is positive because disruption of the interaction leads to a loss-of-function phenotype (Figure 7). Indeed, RIM1 binding to Munc13-1 may serve as a switch to activate the priming apparatus once an appropriate Rab3-bearing vesicle has arrived.

## Experimental Procedures

### Cloning of ubMunc13-2

In order to clone the rat homolog of hMunc13 (GenBank accession number AF020202; Song et al., 1998), we amplified two fragments of the human sequence (bp 216–734 and bp 917–1504), using PCR with human lung cDNA (Clontech) as template. The PCR fragments were subcloned, verified by sequencing (dideoxy chain termination method with dye terminators on an ABI 373 DNA sequencer [Applied Biosystems]), and used as probes to screen a rat lung cDNA library in λgt11 (Clontech) at high stringency. From a total of $3 \times 10^6$ plaques, three positive clones were isolated. The corresponding inserts were subcloned into pBluescript (Stratagene) and sequenced. Two clones encoded a 0.5 kb fragment homologous to the 5′ end of AF020202 (hMunc13). The third clone contained a 1 kb fragment with a short sequence stretch homologous to AF020202 (hMunc13) that was spliced into the rat Munc13-2 sequence at bp 2775 of the Munc13-2 cDNA (GenBank accession number U24071), indicating that the new isoform represents an N-terminal splice variant of Munc13-2. The unknown sequence linking the partial clones isolated in the library screens was amplified from rat lung cDNA (Clontech) using PCR with an oligonucleotide primer pair located in the 5′ untranslated region of the novel variant and in the Munc13-2 sequence 3′ to the putative splice site, respectively. The full-length sequence of the novel Munc13-2 splice variant was assembled from the isolated cDNA clones and overlapping RT–PCR fragments and submitted to GenBank (GenBank accession number AF159706). A full-length mammalian expression vector encoding ubMunc13-2 was constructed in pcDNA3 (pcDNA-ubMunc13-2; Invitrogen) and used for the characterization of antisera. Bacterial expression vectors encoding GST in-frame with various sequences of ubMunc13-2 were constructed in pGEX-KG (Guan and Dixon, 1991). A rabbit polyclonal antibody specifically directed against ubMunc13-2 was generated using the GST-ubMunc13-2(181-408) protein as antigen. A second polyclonal antibody, which detects both Munc13-2 splice variants, was raised against GST-ubMunc13-2(1203-1316) (corresponding to residues 1566–1679 of bMunc13-2; GenBank accession number U24071). Antibodies were generated and purified as described (Augustin et al., 1999a). Antibodies to bMunc13-2 were published previously (Augustin et al., 1999a).

### Yeast Two-Hybrid Screens and Related Methods

A bait vector encoding the LexA DNA binding domain in-frame with residues 1–181 of ubMunc13-2 [pLexN-ubMunc13-2(1-181)] was constructed in pLexN (Vojtek et al., 1993; Betz et al., 1997). Yeast two-hybrid screens using a rat brain cDNA prey library in pVP16-3 and pLexN-ubMunc13-2(1-181) as bait were performed as described elsewhere (Fields and Song, 1989; Betz et al., 1997). Ninety million yeast transformants were screened, and 80 positive clones were isolated and sequenced. Negative control bait vectors were constructed in pLexN.

### Expression Vectors for RIM1 and Munc13-1

Bacterial expression vectors encoding GST in-frame with various sequences of RIM and Munc13-1 were constructed in pGEX-KG (Guan and Dixon, 1991). Mutations in the RIM1 zinc finger were introduced by PCR. Proteins were expressed, purified, and, in the case of GST-Munc13-1(3-317), cleaved with thrombin according to Guan and Dixon (1991). Cleaved Munc13-1(3-317) was further purified by chromatography over a POROS 20 HQ anion exchange column on a BioCAD Perfusion Chromatography Workstation (PerSeptive Biosystems).

### Cosedimentation Assays and Immunoprecipitations

Cosedimentation and immunoprecipitation experiments were performed as described (Betz et al., 1997). In the case of Rab3A/RIM binding, the specificity of the observed interactions was verified by blocking Rab3A binding in the presence of 0.5 mM GDPβS.

### Chromaffin Cell and Hippocampal Neuron Cultures and Electrophysiology

Semliki Forest virus constructs encoding residues 1–1736, 1–451, 162–1736, and 520–1736 of Munc13-1 in-frame with EGFP were constructed in pSFV1 (GIBCO–BRL). Overexpression in chromaffin cells and electrophysiological recordings from chromaffin cells were performed as described (Ashery et al., 1999, 2000). Microisland culture preparation of hippocampal neurons was performed according to a modified version of published procedures (Bekkers and Stevens, 1991; Reim et al., 2001). After 10–14 days in culture, cells were infected with 50 μl of activated Semliki Forest virus according to published protocols (Olkkonen et al., 1993; Ashery et al., 1999, 2000). Data acquisition and analysis were performed as described (Reim et al., 2001). Data are expressed as mean ± standard error. Statistical significance was tested by two-paired Student's t test.

### Antibodies

The following antibodies were used: monoclonal antibodies to RIM (Transduction Laboratories), Munc13-1 (Betz et al., 1998), Rab3A-D (Cl 42.1; Synaptic Systems), and Rab3A (Cl. 42.2; Synaptic Systems), polyclonal antibodies to Munc13-1 (Brose et al., 1995), and bMunc13-2 (Augustin et al., 1999a).

### Acknowledgments

We thank A. Bührmann, T. Hellmann, I. Herfort, and S. Wenger for excellent technical assistance; I. Thanhäuser and F. Benseler for DNA synthesis and sequencing; T. C. Südhof for plasmids, antibodies, and information on the RIM1 knockouts prior to publication; and R. Jahn, E. Neher, and B. Stahl for comments on the manuscript. We are grateful to E. Neher and T. C. Südhof for continued support and advice. This work was supported by grants from the Deutsche Forschungsgemeinschaft (SFB406/A1 to N. B.; Re1092/3-2 to J. R.; Ro1296/6-1 to C. R. and N. B.) and by a EU Network Grant (980236 to U. A.). N. B. and C. R. are Heisenberg Fellows of the Deutsche Forschungsgemeinschaft.

Received February 28, 2001; revised March 19, 2001.

### References

Ashery, U., Betz, A., Xu, T., Brose, N., and Rettig, J. (1999). An efficient method for transfection of adrenal chromaffin cells using the Semliki Forest Virus gene expression system. Eur. J. Cell Biol. *78*, 525–532.

Ashery, U., Varoqueaux, F., Voets, T., Betz, A., Thakur, P., Koch, H., Neher, E., Brose, N., and Rettig, J. (2000). Munc13-1 acts as a priming factor for large dense-core vesicles in bovine chromaffin cells. EMBO J. *19*, 3586–3596.

Augustin, I., Betz, A., Herrmann, C., Jo, T., and Brose, N. (1999a). Differential expression of two novel Munc13 proteins in rat brain. Biochem. J. *337*, 363–371.

Augustin, I., Rosenmund, C., Südhof, T.C., and Brose, N. (1999b). Munc13-1 is essential for fusion competence of glutamatergic synaptic vesicles. Nature *400*, 457–461.

Bekkers, J.M., and Stevens, C.F. (1991). Excitatory and inhibitory autaptic currents in isolated hippocampal neurons maintained in culture. Proc. Natl. Acad. Sci. USA *88*, 7834–7838.

Betz, A., Okamoto, M., Benseler, F., and Brose, N. (1997). Direct interaction of the rat unc-13 homologue Munc13-1 with the N-terminus of syntaxin. J. Biol. Chem. *272*, 2520–2526.

Betz, A., Ashery, U., Rickmann, M., Augustin, I., Neher, E., Südhof, T.C., Rettig, J., and Brose, N. (1998). Munc13-1 is a presynaptic phorbol ester receptor that enhances neurotransmitter release. Neuron *21*, 123–136.

Brose, N., Hofmann, K., Hata, Y., and Südhof, T.C. (1995). Mammalian homologues of C. elegans unc-13 gene define novel family of $C_2$-domain proteins. J. Biol. Chem. *270*, 25273–25280.

Brose, N., Rosenmund, C., and Rettig, J. (2000). Regulation of transmitter release by Unc-13 and its homologues. Curr. Opin. Neurobiol. *10*, 303–311.

Eustance Kohn, R., Duerr, J.S., McManus, J.R., Duke, A., Rakow, T.L., Maruyama, M., Moulder, G., Maruyama, I.N., Barstead, R.J., and Rand, J.B. (2000). Expression of multiple UNC-13 proteins in the *Caenorhabditis elegans* nervous system. Mol. Biol. Cell *11*, 3441–3452.

Fenster, S.D., Chung, W.J., Zhai, R., Cases-Langhoff, C., Voss, B., Garner, A.M., Kaempf, U., Kindler, S., Gundelfinger, E.D., and Garner, C.C. (2000). Piccolo, a presynaptic zinc finger protein structurally related to bassoon. Neuron *25*, 203–214.

Fernandez-Chacon, R., and Südhof, T.C. (1999). Genetics of synaptic vesicle function: towards the complete functional anatomy of an organelle. Annu. Rev. Physiol. *61*, 753–776.

Fields, S., and Song, O. (1989). A novel genetic system to detect protein-protein interactions. Nature *340*, 245–246.

Garcia, E.P., McPherson, P.S., Chilcote, T.J., Takei, K., and De Camilli, P. (1995). rbSec1A and B colocalize with syntaxin 1 and SNAP-25 throughout the axon, but are not in a stable complex with syntaxin. J. Cell Biol. *129*, 105–120.

Gonzalez, L., Jr., and Scheller, R.H. (1999). Regulation of membrane trafficking: structural insights from a Rab/effector complex. Cell *96*, 755–758.

Guan, K.L., and Dixon, J.E. (1991). Eukaryotic proteins expressed in *Escherichia coli*: an improved thrombin cleavage and purification procedure of fusion proteins with glutathion-S-transferase. Anal. Biochem. *193*, 262–267.

Koch, H., Hofmann, K., and Brose, N. (2000). Definition of Munc13-homology domains and characterisation of a novel ubiquitously expressed Munc13-isoform. Biochem. J. *349*, 247–253.

Misura, K.M.S., Scheller, R.H., and Weis, W.I. (2000). Three-dimensional structure of the neuronal-Sec1-syntaxin 1a complex. Nature *404*, 355–362.

Neher, E. (1998). Vesicle pools and $Ca^{2+}$ microdomains: new tools for understanding their roles in neurotransmitter release. Neuron *20*, 389–399.

Olkkonen, V.M., Liljeström, P., Garoff, H., Simons, K., and Dotti, C.G. (1993). Expression of heterologous proteins in cultured rat hippocampal neurons using the Semliki Forest virus vector. J. Neurosci. Res. *35*, 445–451.

Ostermeier, C., and Brünger, A.T. (1999). Structural basis of Rab effector specificity: crystal structure of the small G protein Rab3A complexed with the effector domain of rabphilin-3A. Cell *96*, 363–374.

Ozaki, N., Shibasaki, T., Kashima, Y., Miki, T., Takahashi, K., Ueno, H., Sunaga, Y., Yano, H., Matsuura, Y., Iwanaga, T., et al. (2000). cAMP-GEFII is a direct target of cAMP in regulated exocytosis. Nat. Cell Biol. *2*, 805–811.

Reim, K., Mansour, M., Varoqueaux, F., McMahon, H.T., Südhof, T.C., Brose, N., and Rosenmund, C. (2001). Complexins regulate a late step in $Ca^{2+}$-dependent neurotransmitter release. Cell *104*, 71–81.

Sassa, T., Harada, S., Ogawa, H., Rand, J.B., Maruyama, I.N., and Hosono, R. (1999). Regulation of the UNC-18-Caenorhabditis elegans syntaxin complex by UNC-13. J. Neurosci. *19*, 4772–4777.

Song, Y., Ailenberg, M., and Silverman, M. (1998). Cloning of a novel gene in the human kidney homologous to rat munc13s: its potential role in diabetic nephropathy. Kidney Int. *53*, 1689–1695.

Stahl, B., Chou, J.H., Li, C., Südhof, T.C., and Jahn, R. (1996). Rab3 reversibly recruits rabphilin to synaptic vesicles by a mechanism analogous to raf recruitment by ras. EMBO J. *15*, 1799–1809.

Südhof, T.C. (1995). The synaptic vesicle cycle: a cascade of protein-protein interactions. Nature *375*, 645–653.

Sutton, R.B., Fasshauer, D., Jahn, R., and Brünger, A.T. (1998). Crystal structure of a SNARE complex involved in synaptic exocytosis at 2.4 Å resolution. Nature *395*, 347–353.

tom Dieck, S., Sanmarti-Vila, L., Langnaese, K., Richter, K., Kindler, S., Soyke, A., Wex, H., Smalla, K.H., Kampf, U., Franzer, J.T., et al. (1998). Bassoon, a novel zinc-finger CAG/glutamine-repeat protein selectively localized at the active zone of presynaptic nerve terminals. J. Cell Biol. *142*, 499–509.

Vojtek, A.B., Hollenberg, S.M., and Cooper, J.A. (1993). Mammalian Ras interacts directly with the serine/threonine kinase Raf. Cell *74*, 205–214.

Wang, Y., Okamoto, M., Schmitz, F., Hofmann, K., and Südhof, T.C. (1997). Rim is a putative Rab3 effector in regulating synaptic vesicle fusion. Nature *388*, 593–598.

Wang, X., Kibschull, M., Laue, M.M., Lichte, B., Petrasch-Parwez, E., and Kilimann, M.W. (1999). Aczonin, a 550-kD putative scaffolding protein of presynaptic active zones, shares homology regions with Rim and Bassoon and binds Profilin. J. Cell Biol. *147*, 151–162.

Wang, Y., Sugita, S., and Südhof, T.C. (2000). The RIM/NIM family of neuronal C2-domain proteins: interactions with RAB3 and a new class of neuronal Src homology 3 domain proteins. J. Biol. Chem. *275*, 20033–20044.

Weber, T., Zemelman, B.V., McNew, J.A., Westermann, B., Gmachl, M., Parlati, F., Söllner, T.H., and Rothman, J.E. (1998). SNAREpins: minimal machinery for membrane fusion. Cell *92*, 759–772.

Zucker, R.S. (1996). Exocytosis: a molecular and physiological perspective. Neuron *17*, 1049–1055.

**GenBank Accession Numbers**

The GenBank accession number for the ubMunc13-2 sequence reported in this paper is AF159706.